

Probing Top Quark FCNC $tq\gamma$ and tqZ Couplings at Future Electron-Proton Colliders

O. Cakir

Department of Physics, Ankara University, 06100, Ankara, Turkey

A. Yilmaz

*Department of Electrical and Electronics Engineering,
Giresun University, 28200, Giresun, Turkey*

I. Turk Cakir

*Department of Energy Systems Engineering,
Giresun University, 28200, Giresun, Turkey*

A. Senol, H. Denizli

Department of Physics, Bolu Abant Izzet Baysal University, 14280 Bolu, Turkey

Abstract

The top quark flavor changing neutral current (FCNC) processes are extremely suppressed within the Standard Model (SM) of particle physics. However, they could be enhanced in a new physics model Beyond the Standard Model (BSM). The top quark FCNC interactions would be a good test of new physics at present and future colliders. Within the framework of the BSM models, these interactions can be described by an effective Lagrangian. In this work, we study $tq\gamma$ and tqZ effective FCNC interaction vertices through the process $e^-p \rightarrow e^-Wq + X$ at future electron proton colliders, projected as Large Hadron electron Collider (LHeC) and Future Circular Collider-hadron electron (FCC-he). The cross sections for the signal have been calculated for different values of parameters λ_q for $tq\gamma$ vertices and κ_q for tqZ vertices. Taking into account the relevant background we estimate the attainable range of signal parameters as a function of the integrated luminosity and present contour plots of couplings for different significance levels including detector simulation.

PACS numbers: 14.65.Ha Top quarks, 12.39.-x Phenomenological quark models, 13.87.Ce Production.

Keywords: Top, FCNC, Electron-Proton, Colliders.

I. INTRODUCTION

Within the framework of the Standard Model (SM) of particle physics, the top quark (with mass $m_t \sim 173$ GeV) being the heaviest of fundamental fermions decays to a bottom quark and a W boson (most frequently) while its decays to light down type quarks are suppressed due to the Cabibbo-Kobayashi-Maskawa (CKM) matrix [1, 2]. It is also known that flavor changing neutral current (FCNC) transitions in the up-sector or down-sector are absent at tree level. Furthermore, these transitions at the loop level are highly suppressed due to the Glashow-Iliopoulos-Maiani (GIM) mechanism [3]. From both theoretical and experimental perspective, studying the top quark FCNC interactions is an important component of the top quark physics program. The top quark FCNC interactions at loop level are extremely suppressed in the SM, with branching ratios $\text{BR}(t \rightarrow c\gamma) \sim 10^{-14}$, $\text{BR}(t \rightarrow cZ) \sim 10^{-14}$, $\text{BR}(t \rightarrow cg) \sim 10^{-12}$ and $\text{BR}(t \rightarrow cH) \sim 10^{-15}$, and the branchings are about one order smaller for top to up quark transitions, which are well beyond the current sensitivity of the Large Hadron Collider (LHC) experiments. However, these decay modes could be enhanced in some extensions of the SM, for instance due to the presence of new virtual particles in the loops. Therefore, top sector is considered to be powerful probe for new physics beyond the SM.

The ATLAS and CMS experiments have significantly improved previous exclusion limits on the top quark FCNC couplings. The experimental 95% confidence level (C.L.) upper limits on the branching fractions of the top quark FCNC decays obtained at the LHC are summarized as follows: $\text{BR}(t \rightarrow ug) \leq 4.0 \times 10^{-5}$, $\text{BR}(t \rightarrow cg) \leq 2.0 \times 10^{-4}$ [4]; $\text{BR}(t \rightarrow u\gamma) \leq 1.3 \times 10^{-4}$, $\text{BR}(t \rightarrow c\gamma) \leq 1.7 \times 10^{-3}$ [5]; $\text{BR}(t \rightarrow uH) \leq 2.4 \times 10^{-3}$ and $\text{BR}(t \rightarrow cH) \leq 2.2 \times 10^{-3}$ [6]. Recently, a combined result for the tqZ couplings (through anomalous tZ production) has been improved to give the limits $\text{BR}(t \rightarrow uZ) \leq 2.2 \times 10^{-4}$ and $\text{BR}(t \rightarrow cZ) \leq 4.9 \times 10^{-4}$ [7]. At the high luminosity Large Hadron Collider (HL-LHC) with $L_{int} = 3 \text{ ab}^{-1}$ the limits on the top FCNC are estimated to be $\text{BR}(t \rightarrow q\gamma) \leq 2.5 \times 10^{-5}$ [8], $\text{BR}(t \rightarrow uZ) \leq 4.3 \times 10^{-5}$ and $\text{BR}(t \rightarrow cZ) \leq 5.8 \times 10^{-5}$ [9] at 95% C.L.

Phenomenologically, the sensitivities to the top quark FCNC interactions have been estimated on the branching ratio $\text{BR}(t \rightarrow uZ/u\gamma) \simeq 10^{-5}$ for the HL-LHC with $\sqrt{s} = 14$ TeV and $L_{int} = 3 \text{ ab}^{-1}$, and the branching ratio $\text{BR}(t \rightarrow uZ/u\gamma) \simeq 10^{-6}$ for Future Circular Collider- hadron hadron (FCC-hh) with $\sqrt{s} = 100$ TeV and $L_{int} = 10 \text{ ab}^{-1}$ in Ref. [10],

however the bounds have been estimated an order of magnitude small for $\text{BR}(t \rightarrow cZ/c\gamma)$.

The future hadron electron collider projects currently under consideration are the Large Hadron electron Collider (LHeC) [11] and Future Circular Collider-hadron electron (FCC-he) [12]. The LHeC comprises a 60 GeV electron beam that will collide with the 7 TeV proton beam of LHC, having an integrated luminosity of $L_{int} = 100 \text{ fb}^{-1}$ per year, and planning to reach 1 ab^{-1} over the years. On the other hand, the FCC-he mode is considered to be realized by accelerating electrons up to 60 GeV and colliding them with the proton beam at the energy of 50 TeV. Recently, the new physics capability and potential of the projected ep colliders have been reported in Refs. [11–15].

In this work, we study the process $e^-p \rightarrow e^-Wq+X$ including $tq\gamma$ and tqZ effective FCNC interaction vertices at future hadron electron colliders, namely LHeC and FCC-he. The effective Lagrangian is introduced and used in Section II to calculate the top quark FCNC decay widths $\Gamma(t \rightarrow q\gamma)$ and $\Gamma(t \rightarrow qZ)$ and the branching ratios. The cross sections for the signal have been calculated for different values of parameters λ_q for $tq\gamma$ vertices and κ_q for tqZ vertices. We estimate the attainable range of top quark FCNC parameters depending on the integrated luminosity of the future ep colliders in section III. The signal and background analysis including effects from detector fast simulation have been performed, and the contour plots of couplings κ_q and λ_q at different significance levels have been presented. Finally, we summarize our results and conclude on the better limits of the top FCNC branchings.

II. TOP QUARK FCNC $tq\gamma$ AND tqZ INTERACTIONS

At the electron-proton collision environment, top quark anomalous FCNC interactions in the $tq\gamma$ and tqZ vertices can be described in a model independent effective Lagrangian

$$L_{eff} = \frac{g_e}{2m_t} \bar{t} \sigma^{\mu\nu} (\lambda_u^L P_L + \lambda_u^R P_R) u A_{\mu\nu} + \frac{g_e}{2m_t} \bar{t} \sigma^{\mu\nu} (\lambda_c^L P_L + \lambda_c^R P_R) c A_{\mu\nu} \\ + \frac{g_W}{4c_W m_Z} \bar{t} \sigma^{\mu\nu} (\kappa_u^L P_L + \kappa_u^R P_R) u Z_{\mu\nu} + \frac{g_W}{4c_W m_Z} \bar{t} \sigma^{\mu\nu} (\kappa_c^L P_L + \kappa_c^R P_R) c Z_{\mu\nu} + h.c. \quad (1)$$

where $g_e(g_W)$ is the electromagnetic (weak) coupling constant; c_W is the cosine of weak mixing angle; $\lambda_q^{L(R)}$ and $\kappa_q^{L(R)}$ are the strengths of anomalous top FCNC $tq\gamma$ and tqZ couplings (where $q = u, c$), the values of these couplings vanish at the lowest order in the SM; $P_{L(R)}$ denotes the left (right) handed projection operators. The photon field strength tensor is $A_{\mu\nu}$ and Z boson field strength tensor is $Z_{\mu\nu}$, and the anti-symmetric tensor $\sigma^{\mu\nu} = \frac{i}{2}[\gamma^\mu, \gamma^\nu]$.

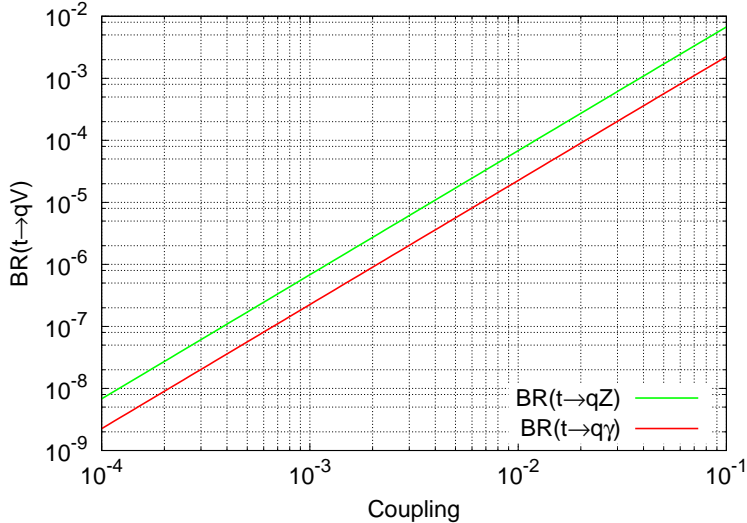


FIG. 1. Branching ratios for decay channels $t \rightarrow q\gamma$ and $t \rightarrow qZ$ depending on the FCNC coupling.

The effective Lagrangian is used to calculate both decay widths (for the channels $t \rightarrow q\gamma$ and $t \rightarrow qZ$) and production cross sections.

In addition to the usual decay channel $t \rightarrow W^+b$, the top quark can also decay into up-type quarks (u or c) associated with a vector boson via FCNC as given in Eq. 1. Considering only the SM decay width and the FCNC interactions with electroweak neutral gauge bosons, the top quark decay width (Γ_t) can be written as

$$\begin{aligned} \Gamma_t = & \Gamma(t \rightarrow W^+b) + \Gamma(t \rightarrow W^+s) + \Gamma(t \rightarrow W^+d) \\ & + \Gamma(t \rightarrow cZ) + \Gamma(t \rightarrow uZ) + \Gamma(t \rightarrow c\gamma) + \Gamma(t \rightarrow u\gamma) \end{aligned} \quad (2)$$

The dominant SM decay mode of top quark is $t \rightarrow W^+b$, the decay width for this mode is given as

$$\Gamma(t \rightarrow W^+b) = \frac{\alpha |V_{tb}|^2 m_t^3}{16s_W^2 m_W^2} (1 - 3m_W^4/m_t^4 + 2m_W^6/m_t^6) \quad (3)$$

at the leading order (LO), and it is improved to the next to leading order (NLO) expression as given in Ref. [16]. The ratios of the SM decay widths are calculated as $\Gamma(t \rightarrow W^+s)/\Gamma(t \rightarrow W^+b) \simeq |V_{ts}|^2/|V_{tb}|^2 \simeq 1.495 \times 10^{-3}$ and $\Gamma(t \rightarrow W^+d)/\Gamma(t \rightarrow W^+b) \simeq |V_{td}|^2/|V_{tb}|^2 \simeq 6.318 \times 10^{-5}$ [17]. The top quark FCNC partial decay widths are

$$\Gamma(t \rightarrow q\gamma) = \frac{\alpha}{4}(\lambda_{qL}^2 + \lambda_{qR}^2)m_t \quad (4)$$

for the $t \rightarrow q\gamma$ channel. While, the other partial decay widths are

$$\Gamma(t \rightarrow qZ) = \frac{\alpha}{32s_W^2c_W^2m_Z^2}(\kappa_{qL}^2 + \kappa_{qR}^2)m_t^3(1 - m_Z^2/m_t^2)(2 - m_Z^2/m_t^2 - m_Z^4/m_t^4) \quad (5)$$

for the $t \rightarrow qZ$ channel. The branching ratios for $t \rightarrow q\gamma$ and $t \rightarrow qZ$ decay channels depending on the FCNC $tq\gamma$ and tqZ couplings are shown in Fig. 1.

III. SENSITIVITY AT FUTURE EP COLLIDERS

The production subprocess ($e^-q \rightarrow e^-W^+b$, where $q = u, c$) including signal diagrams with $tq\gamma$ and tqZ interaction vertices is presented in Fig. 2. The similar diagrams for the subprocess ($e^-\bar{q} \rightarrow e^-W^-\bar{b}$) have also been included in the calculation. The cross sections for the process $e^-p \rightarrow e^-W^\pm q + X$ at different values of couplings κ_q and λ_q in the range of (0.00 – 0.05) at LHeC and FCC-he are given in Table I and Table II, respectively. The cross section increases when the coupling parameters κ_q and λ_q grow in the interested range. We plot the contours using Table I and Table II to estimate the sensitivity to FCNC coupling parameters, the contour lines correspond to different values of the signal cross sections (where $\Delta\sigma$ denotes the signal cross section (in pb) when the interfering background cross section is subtracted from the total cross section) as shown in Fig. 3 and Fig. 4 for LHeC and FCC-he, respectively. For a cross section value of the signal the sensitivity to coupling parameter λ_q is higher than the coupling parameter κ_q .

The process $e^-p \rightarrow e^-W^\pm q + X$ includes both the signal and the background interfering with the signal. We calculate the cross sections for this process to normalize the distributions from the signal and background events. We take into account the main background (B1: $e^-W^\pm q$) and include other background (B2: e^-Zq) which contain at least three jets and one electron in the final state. Here, QCD multijet backgrounds are not included in the analysis of top quark FCNC $tq\gamma$ and tqZ interactions.

In our calculations, we produce signal and background events by using MadGraph 5_aMC@NLO [18], with an effective Lagrangian implementation through FeynRules [19] for

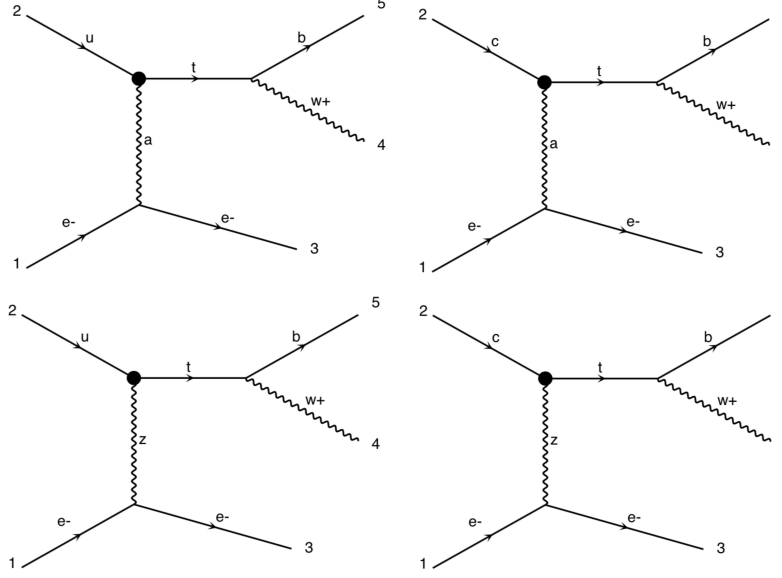


FIG. 2. Diagrams including top quark FCNC $tq\gamma$ and tqZ interaction vertices.

TABLE I. The cross section values (in pb) for process $e^-p \rightarrow e^-W^\pm q + X$ at LHeC depending on different values of the couplings.

LHeC	$\lambda_q = 0.00$	$\lambda_q = 0.01$	$\lambda_q = 0.02$	$\lambda_q = 0.03$	$\lambda_q = 0.05$
$\kappa_q = 0.00$	2.3000	2.3094	2.3365	2.3805	2.5213
$\kappa_q = 0.01$	2.3043	2.3136	2.3236	2.3852	2.5268
$\kappa_q = 0.02$	2.3135	2.3406	2.3505	2.3957	2.5387
$\kappa_q = 0.03$	2.3286	2.3390	2.3666	2.4123	2.5559
$\kappa_q = 0.05$	2.3782	2.3885	2.4173	2.4639	2.6082

TABLE II. The cross section values (in pb) for process $e^-p \rightarrow e^-W^\pm q$ at FCC-he depending on different values of the couplings.

FCC-he	$\lambda_q = 0.00$	$\lambda_q = 0.01$	$\lambda_q = 0.02$	$\lambda_q = 0.03$	$\lambda_q = 0.05$
$\kappa_q = 0.00$	8.6100	8.6421	8.7275	8.8737	9.3411
$\kappa_q = 0.01$	8.6251	8.6574	8.7445	8.8914	9.3636
$\kappa_q = 0.02$	8.6646	8.6956	8.7899	8.9344	9.4088
$\kappa_q = 0.03$	8.7324	8.7659	8.8518	9.0031	9.4776
$\kappa_q = 0.05$	8.9341	8.9725	9.0690	9.2270	9.7070

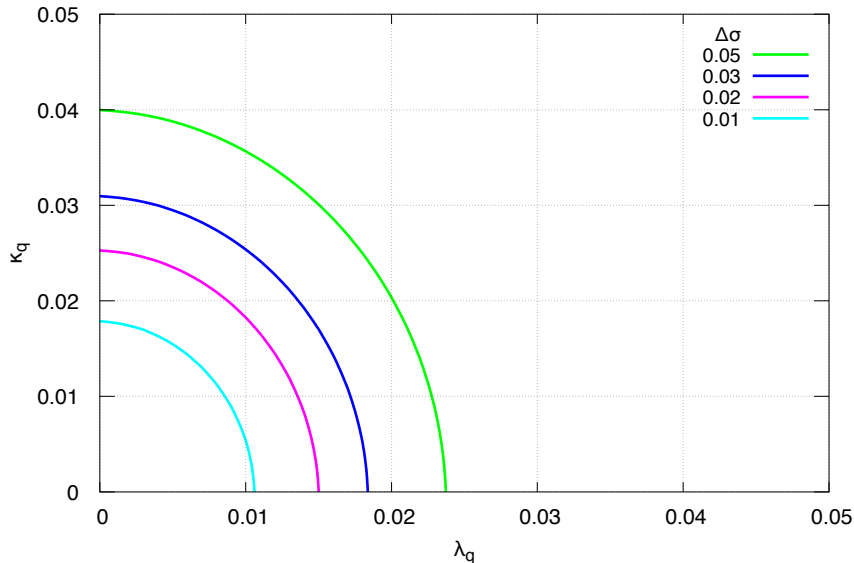


FIG. 3. Contour plot for the top quark FCNC couplings κ_q and λ_q depending on the values (in pb) of signal cross sections at LHeC.

the signal. Afterwards the parton showering and detector fast simulations are carried out with Pythia 6 [20] and Delphes 3.4 [21], respectively.

The kinematical distributions for signal and background are given in Fig. 5 for LHeC and in Fig. 6 for FCC-he. The transverse momentum (p_T) (on the left) and rapidity (η) (on the right) distributions of the leading jet, sub-leading jet and sub-sub-leading jets are presented in these figures. These distributions are obtained after preselection of the events. For the analysis of signal and background events, we also apply analysis cuts after the generator level pre-selection. In order to select signal events we require having one electron and three jets ordered according to the highest transverse momentum p_T . Since there is an energy asymmetry in the electron-proton collisions, the jets from the process mainly peaks in the backward region, hence the pseudo-rapidity range for jets is taken as $-4 < \eta < 0$ in the analysis. The transverse momentum p_T and pseudo-rapidity η distributions of signal and main background have quite similar behaviour since we deal with small couplings for the signal and we take into account the interference of signal and background as well. In Fig. 7 and Fig. 8, the kinematical distributions (p_T and η) of electron in the events are depicted. One of the specific aspects of the signal is the occurrence of the high p_T electron in the

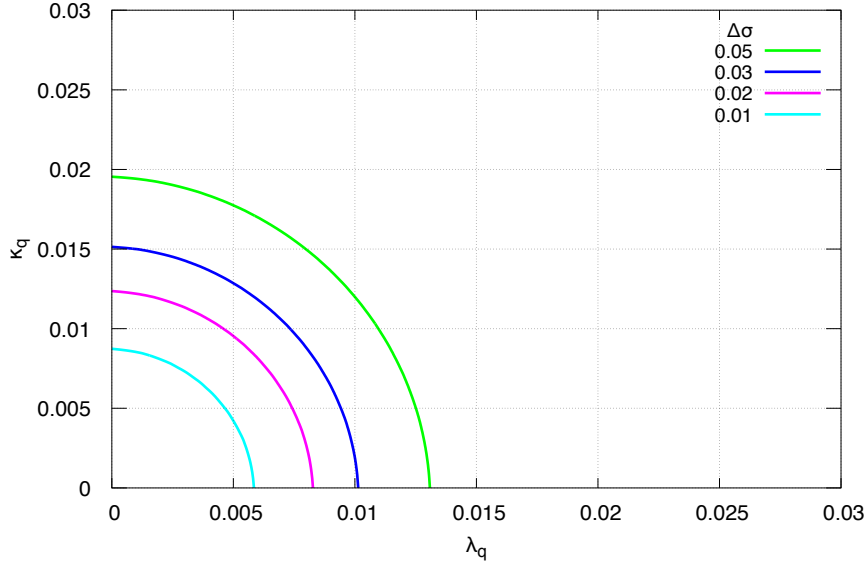


FIG. 4. Contour plot for the top quark FCNC couplings κ_q and λ_q depending on the values (in pb) of signal cross section at FCC-he.

central η region.

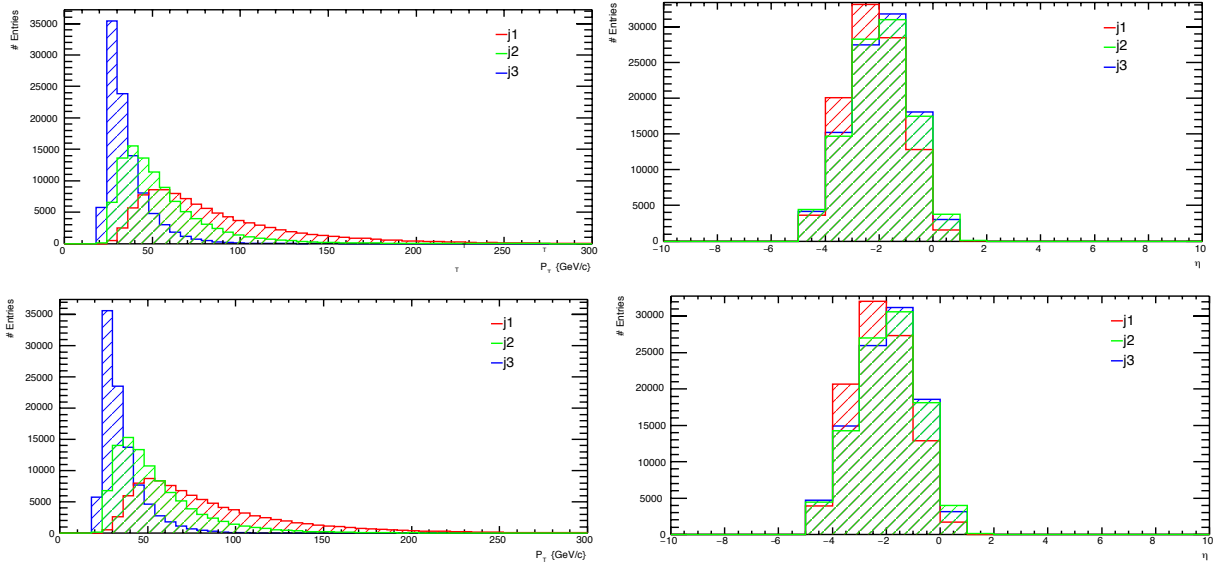


FIG. 5. Transverse momentum (p_T) and pseudo-rapidity (η) distributions of three jets from the process $e^-p \rightarrow e^-W^\pm q + X$ which includes both the interfering background and signal for $\kappa_q = \lambda_q = 0.05$ at the LHeC. The plots in the second line show the distributions for only main background.

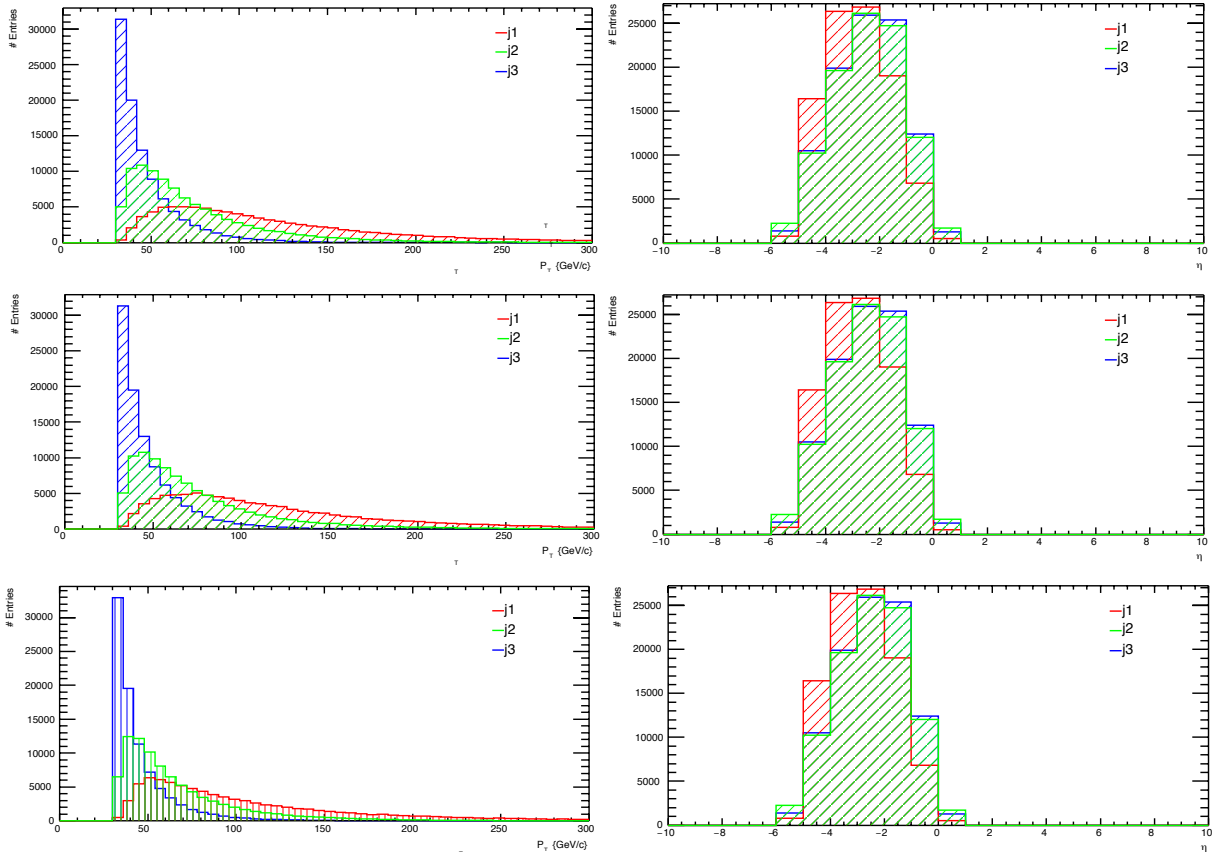


FIG. 6. Transverse momentum and pseudo-rapidity distributions of three jets from the process $e^-p \rightarrow e^-W^\pm q + X$ which includes both the interfering background and signal for $\kappa_q = \lambda_q = 0.05$ at the FCC-he. The plots on the second line and third line show the distributions for only background (B1) and (B2), respectively.

In the analysis, we require at least three jets and one electron in the events, one of the jets should be b -tagged with leading jet $p_T(j) > 40$ GeV and other jets having $p_T(j) > 30$ GeV and $|\eta(j)| < 2.5$, the electron with $p_T(e) > 20$ GeV and $|\eta(e)| < 2.5$ as the cut flow given in Table III. Further steps in the cut flow table include invariant mass intervals for selecting events for the analysis.

The cut efficiencies have been calculated after pre-selection for signal and background as shown in Fig. 9 for LHeC and Fig. 10 for FCC-he. We have larger cut efficiencies for higher values of the FCNC couplings. Fig. 9 shows that the cut efficiency for the background changes from 6% to 1% for Cut-1 to Cut-5, whereas the cut efficiencies for the signal decrease from 11% to 3.2% for couplings $\kappa_q = \lambda_q = 0.05$.

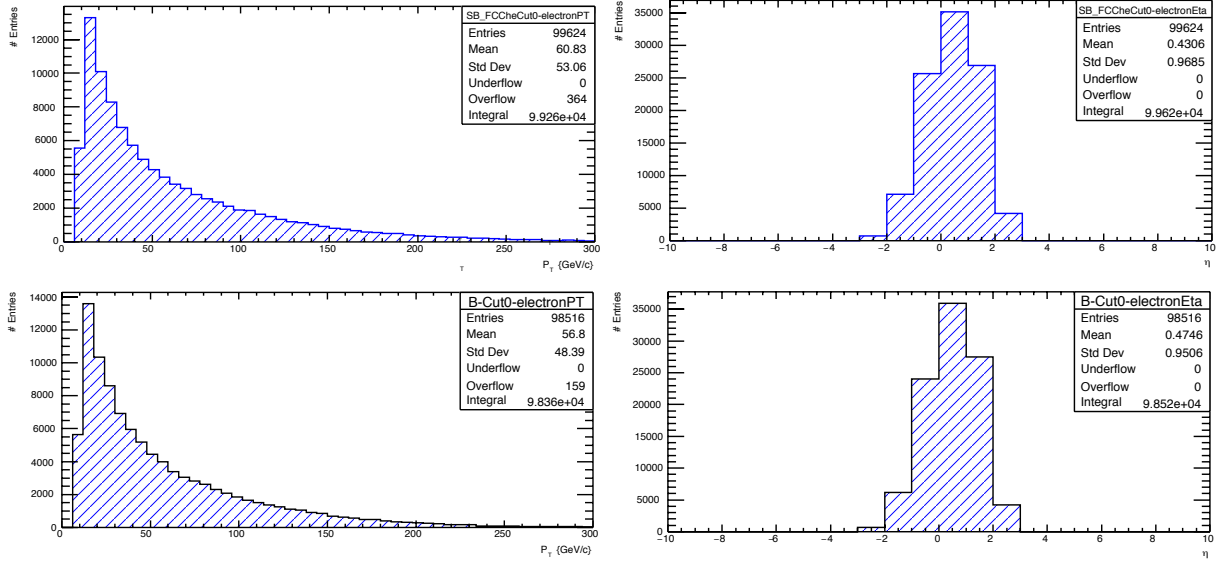


FIG. 7. Transverse momentum and pseudo-rapidity distributions of electron from the process $e^-p \rightarrow e^-W^\pm q + X$ which includes both the interfering background and signal for $\kappa_q = \lambda_q = 0.05$ at the LHeC.

TABLE III. Preselection and a set of cuts for the analysis of signal and background events.

Cuts	Definition
Cut-0	Preselection: $N_{jets} \geq 3$ and $N_e \geq 1$
Cut-1	b -tag: one b -tagged jet (j_b)
Cut-2	Transverse momentum: $p_T(j_2, j_3) > 30$ GeV and $p_T(j_b) > 40$ GeV and $p_T(e) > 20$ GeV
Cut-3	Pseudo-rapidity: $-4 < \eta(j_b, j_2, j_3) < 0$ and $ \eta(e) < 2.5$
Cut-4	W boson mass: $50 < M_{inv}^{rec}(j_2, j_3) < 100$ GeV
Cut-5	Top quark mass: $130 < M_{inv}^{rec}(j_b, j_2, j_3) < 200$ GeV

After Cut-5, the number of events for background and signal (different values of couplings κ_q and λ_q) are given in Table IV for LHeC and in Table V and Table VI for FCC-he with an integrated luminosity of 100 fb^{-1} . For the coupling parameters $\kappa_q = \lambda_q = 0.05$ we obtain the number of events 2153, while the background events are 508. Thus, the signal gives an enhancement factor of 3.24 over the background for $\kappa_q = \lambda_q = 0.05$, whereas this factor is 0.17 for $\kappa_q = \lambda_q = 0.01$. For each cut step the number of events can be obtained from Table IV with the relative cut efficiency factors from Fig. 9 and Fig. 10.

We plot the invariant mass distribution of top quark reconstructed from three jets (one

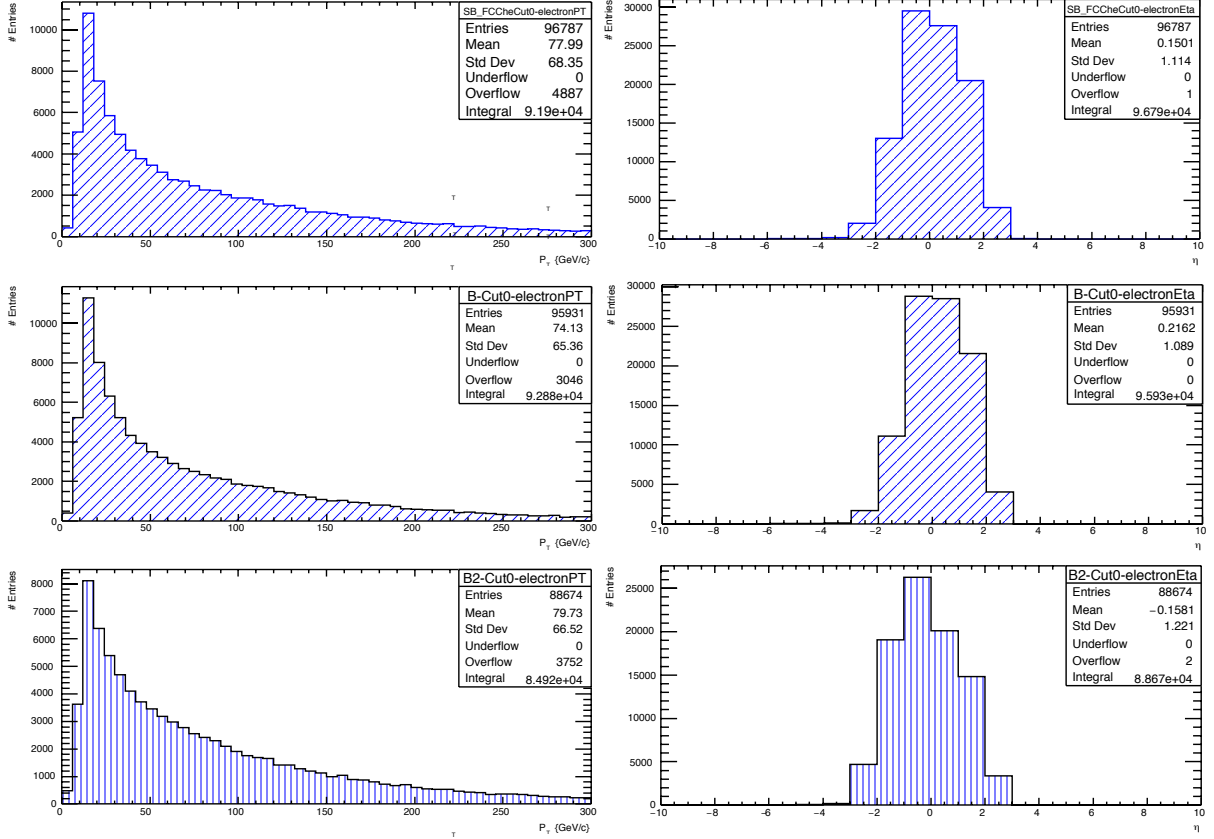


FIG. 8. Transverse momentum and pseudo-rapidity distributions of electron from the process $e^-p \rightarrow e^-W^\pm q + X$ which includes both the interfering background and signal for $\kappa_q = \lambda_q = 0.05$ at the FCC-he. The plots in the second and third line shows the distributions for only background B1 and B2, respectively.

TABLE IV. The number of events for background (where $\kappa_q = 0$ and $\lambda_q = 0$) and signal (where $\kappa_q \neq 0$ and $\lambda_q \neq 0$) with different FCNC couplings κ_q and λ_q at LHeC with $L_{int} = 100 \text{ fb}^{-1}$.

LHeC	$\lambda_q = 0.00$	$\lambda_q = 0.01$	$\lambda_q = 0.02$	$\lambda_q = 0.03$	$\lambda_q = 0.05$
$\kappa_q = 0.00$	508	558	670	894	1469
$\kappa_q = 0.01$	549	595	741	901	1624
$\kappa_q = 0.02$	622	646	779	971	1633
$\kappa_q = 0.03$	721	765	834	1113	1841
$\kappa_q = 0.05$	1037	1120	1256	1514	2153

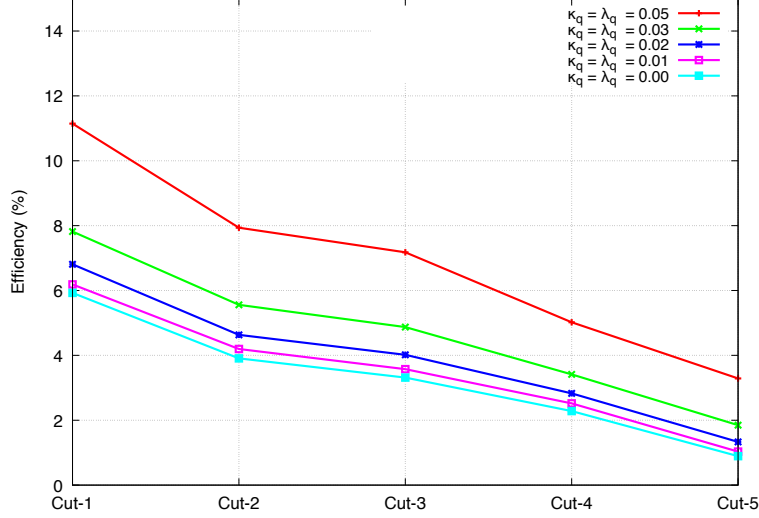


FIG. 9. Efficiency plot for the cuts applied at each step for the analysis of signal and background at LHeC.

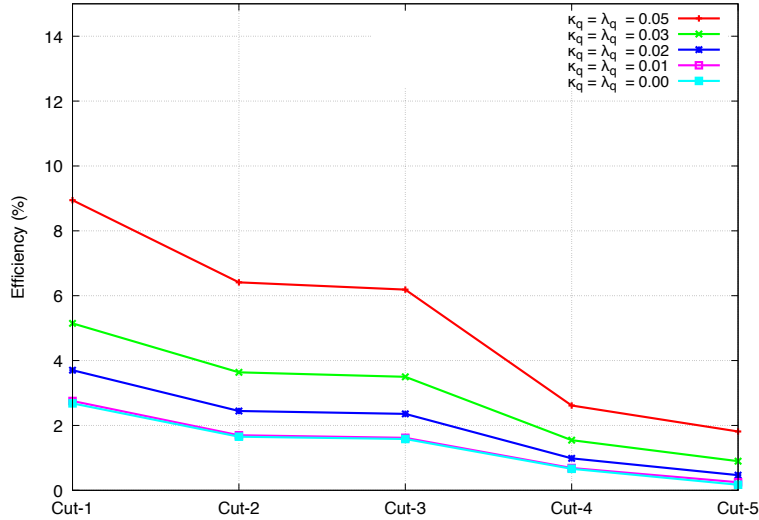


FIG. 10. Efficiency plot for the cuts applied at each step for the analysis of signal and background at FCC-he.

of them is b -tagged) for different coupling scenarios (a) $\lambda_q = 0.0, \kappa_q = 0.05$, (b) $\lambda_q = 0.05, \kappa_q = 0.0$ and (c) $\lambda_q = 0.05, \kappa_q = 0.05$) as shown in Fig. 11 for LHeC and Fig. 12 for FCC-he. The ratio of the $S + B$ and B is more enhanced at top mass for equal coupling scenario (c) when it is compared with the other scenarios (a) and (b) as seen from Fig. 11 and Fig. 12.

In order to quantify statistical significance (SS), we calculate signal (S) and background

TABLE V. The number of events for background ($B1$ when $\kappa_q = \lambda_q = 0$) and signal+background ($S + B1$ when $\kappa_q \neq 0$ and $\lambda_q \neq 0$) with FCNC couplings κ_q and λ_q at FCC-he with $L_{int} = 100$ fb $^{-1}$.

FCC-he	$\lambda_q = 0.00$	$\lambda_q = 0.01$	$\lambda_q = 0.02$	$\lambda_q = 0.03$	$\lambda_q = 0.05$
$\kappa_q = 0.00$	231	269	462	809	1765
$\kappa_q = 0.01$	259	334	491	834	1818
$\kappa_q = 0.02$	421	466	647	998	1932
$\kappa_q = 0.03$	576	703	915	1286	2227
$\kappa_q = 0.05$	1292	1407	1652	1921	2844

TABLE VI. The number of events for the background ($B = B1 + B2$ when $\kappa_q = \lambda_q = 0$) and signal+background ($S + B$ when $\kappa_q \neq 0$ and $\lambda_q \neq 0$) with FCNC couplings κ_q and λ_q at FCC-he with $L_{int} = 100$ fb $^{-1}$.

FCC-he	$\lambda_q = 0.00$	$\lambda_q = 0.01$	$\lambda_q = 0.02$	$\lambda_q = 0.03$	$\lambda_q = 0.05$
$\kappa_q = 0.00$	380	419	612	959	19145
$\kappa_q = 0.01$	408	483	641	983	1968
$\kappa_q = 0.02$	570	615	796	1148	2082
$\kappa_q = 0.03$	726	852	1065	1435	2377
$\kappa_q = 0.05$	1441	1556	1802	2070	2994

(B) events after final cut. Here the SS is defined by

$$SS = \sqrt{2[(S + B) \ln(1 + \frac{S}{B}) - S]} \quad (6)$$

The SS values depending on the integrated luminosity ranging from 1 fb $^{-1}$ to 1 ab $^{-1}$ at the LHeC are presented in Fig. 13 for the coupling scenarios (a) $\lambda_q = 0.0, \kappa_q = 0.05$, (b) $\lambda_q = 0.05, \kappa_q = 0.0$ and (c) $\lambda_q = 0.05, \kappa_q = 0.05$). The significance corresponding to 2σ , 3σ and 5σ lines (dotted) are also shown in these figures. In Fig. 14, the SS values depending on the integrated luminosity ranging from 1 fb $^{-1}$ to 1 ab $^{-1}$ at the FCC-he are presented for these coupling scenarios with the 2σ , 3σ and 5σ significances.

Using the corresponding statistical significances, we fit the significance as a function of two parameters κ_q and λ_q at the integrated luminosity of 1 fb $^{-1}$ and 1 ab $^{-1}$. We obtain

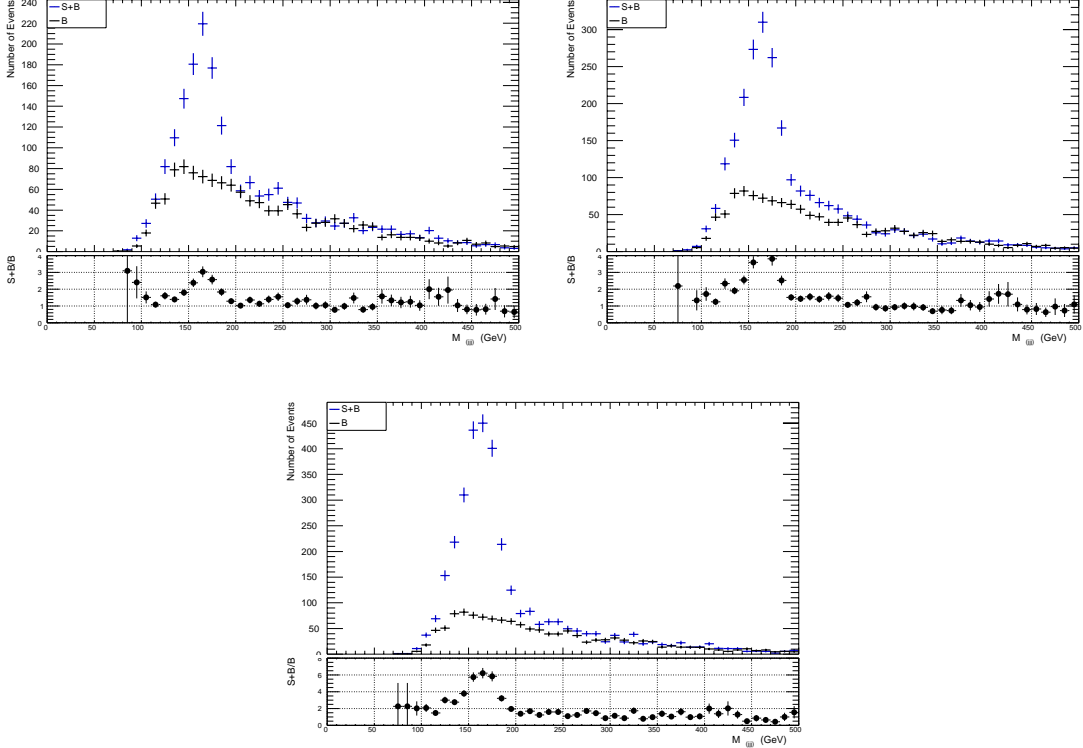


FIG. 11. Invariant mass distributions of three jets (one of the jets is required as b -jet) for the signal + background (S+B) where B is the main background at LHeC. First plot is for $\lambda_q = 0$, $\kappa_q = 0.05$, second plot is for $\lambda_q = 0.05$, $\kappa_q = 0$ and third plot is for $\lambda_q = \kappa_q = 0.05$.

contour lines from the fit procedure. In Fig. 15 and Fig. 16, we estimate the reach for couplings κ_q and λ_q corresponding to 2σ , 3σ and 5σ significance for integrated luminosity of 100 fb^{-1} and 1 ab^{-1} at the LHeC and FCC-he, respectively. We obtain the 2σ significance for the couplings $\kappa_q = 0.014$, $\lambda_q = 0.012$ and $\kappa_q = 0.008$, $\lambda_q = 0.007$ at LHeC with the integrated luminosities 100 fb^{-1} and 1 ab^{-1} , respectively. The sensitivities to the couplings are enhanced at FCC-he as the obtained values $\kappa_q = 0.008$, $\lambda_q = 0.006$ and $\kappa_q = 0.0037$, $\lambda_q = 0.0025$ for $L_{int} = 100 \text{ fb}^{-1}$ and 1 ab^{-1} , respectively.

The limits on couplings can be translated into the branching ratio via Fig. 1. We find the upper limits on branching ratio $\text{BR}(t \rightarrow qZ) \leq 4.0 \times 10^{-5}$ and $\text{BR}(t \rightarrow qZ) \leq 1.0 \times 10^{-5}$ at 2σ significance level for $L_{int} = 1 \text{ ab}^{-1}$ at LHeC and FCC-he, respectively. The HL-LHC will produce a large number of top quarks, which also provide opportunity to search for FCNC processes to improve existing constraints on the branching ratios $\text{BR}(t \rightarrow qZ) < 10^{-5}$ with the upgraded LHC experiments. We find better limits when compared to the current

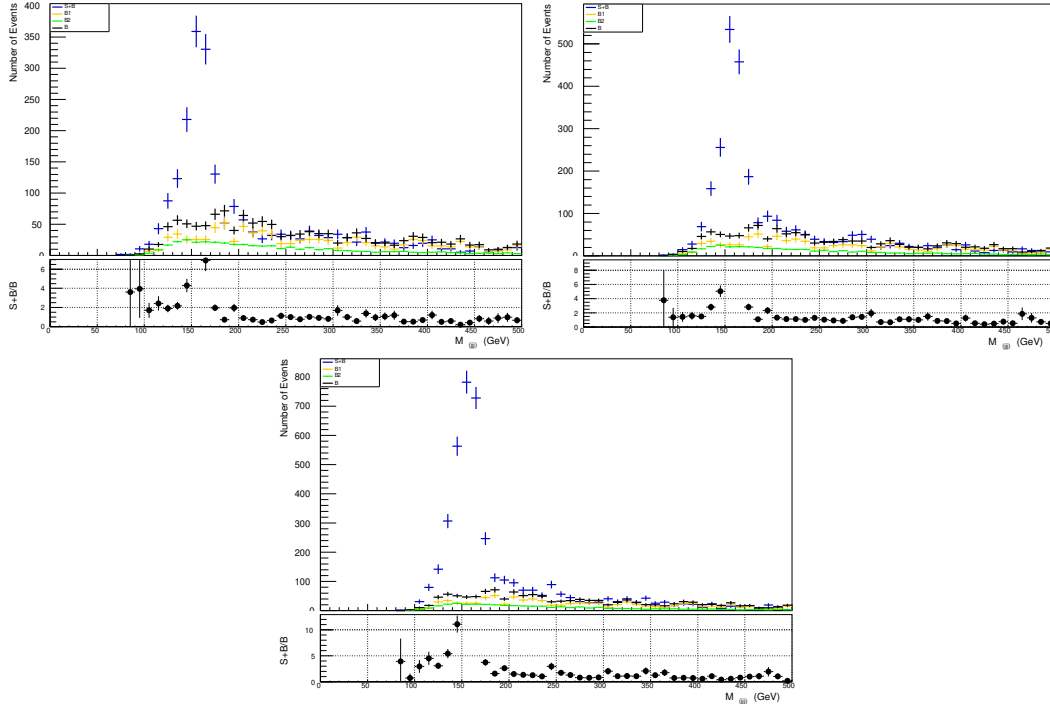


FIG. 12. Invariant mass distributions of three jets (one of the jets is required as b -jet) for the signal + background (S+B) where background B includes background B1 and B2 at FCC-he. First plot is for $\lambda_q = 0$, $\kappa_q = 0.05$, second plot is for $\lambda_q = 0.05$, $\kappa_q = 0$ and third plot is for $\lambda_q = \kappa_q = 0.05$.

experimental limits and estimations at HL-LHC. In our previous studies Refs. [13] and [14], we have obtained the limits on the top quark FCNC $tq\gamma$ couplings depending on the integrated luminosity of future ep colliders. As a complementary to these studies, here we have analyzed both $tq\gamma$ and tqZ couplings in three different scenarios and sensitivities to the couplings κ_q and λ_q . Finally, the summary of branching ratio limits for top quark FCNC decay channels at the future ep experiments (LHeC and FCC-he) for the luminosity projection of 1 ab^{-1} is presented in Fig. 17.

IV. CONCLUSION

The top quark FCNC interactions are important probes for new physics beyond the SM. It is also worth to mention that the analysis include the signal and background interference effects. The physics potential of future ep colliders LHeC and FCC-he for probing new physics through top FCNC is promoted with their expected complementarity to the future

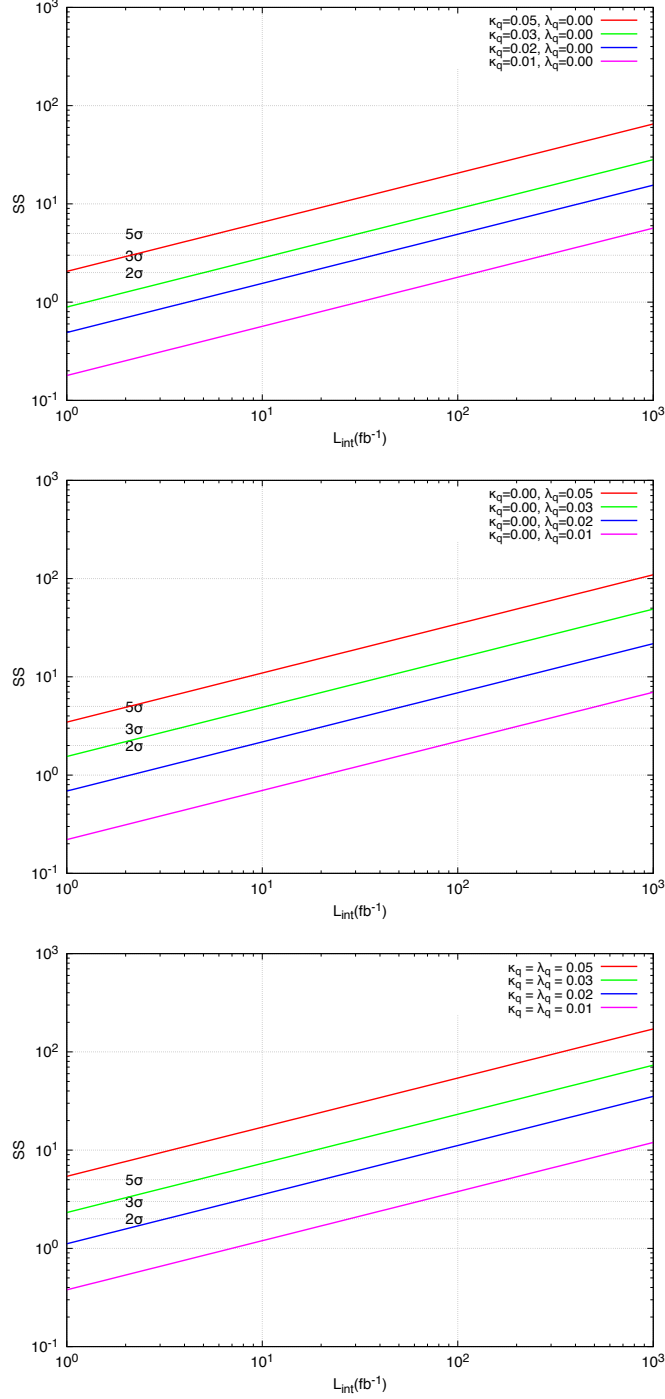


FIG. 13. The statistical significance (SS) for the integrated luminosity ranging from 100 fb^{-1} to 1 ab^{-1} at the LHeC. It includes the contribution from the main backgrounds on the predicted results. First panel shows SS plot for $\lambda_q = 0$ while κ_q changes, second panel is for $\kappa_q = 0$ while λ_q changes, and third panel shows equal coupling scenario $\kappa_q = \lambda_q$.

lepton and hadron colliders. A better sensitivity have been achieved for the $tq\gamma$ and tqZ

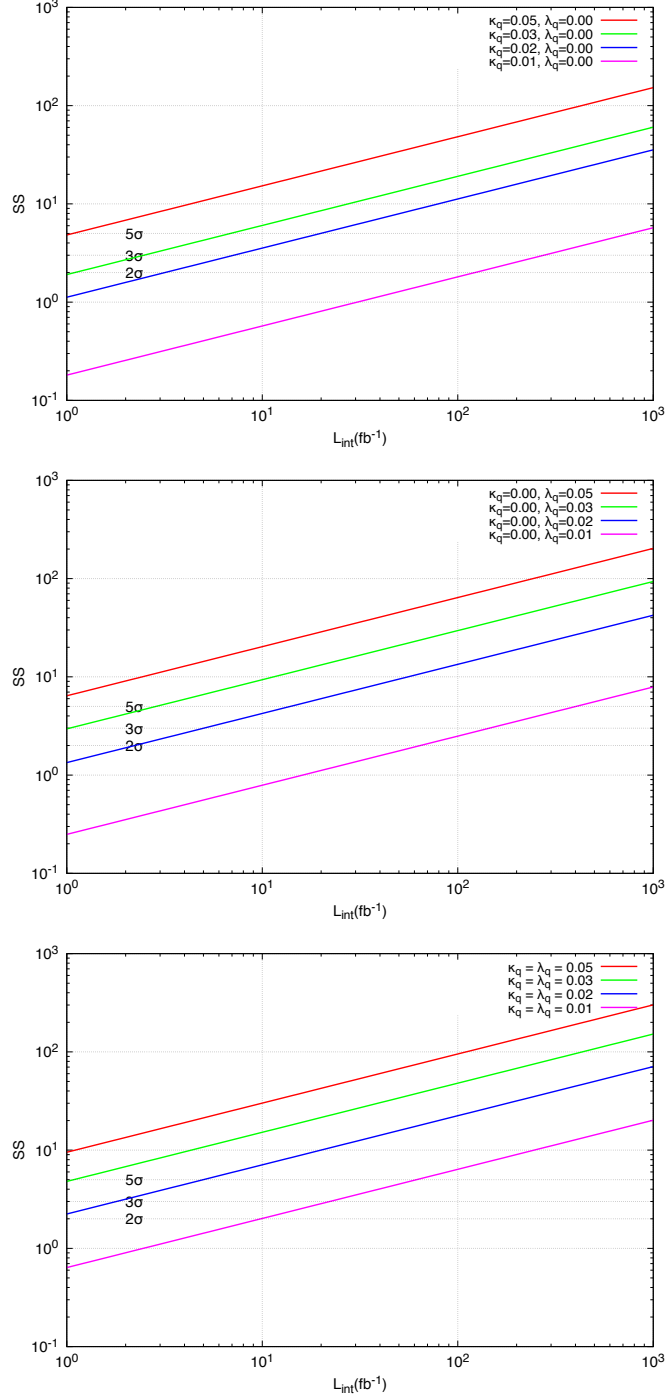


FIG. 14. The statistical significance (SS) for integrated luminosity ranging from 1 fb^{-1} to 1 ab^{-1} at the FCC-he. It includes the contribution from the main background on the predicted results. First panel shows SS plot for $\lambda_q = 0$ while κ_q changes, second panel is for $\kappa_q = 0$ while λ_q changes, and third panel shows equal coupling scenario.

FCNC couplings at the LHeC with the center of mass energy of 1.3 TeV and integrated

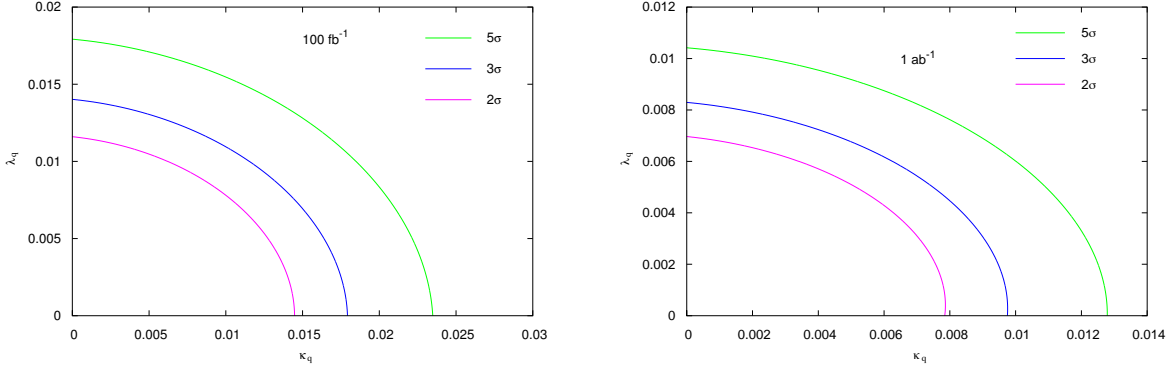


FIG. 15. The reach of proposed couplings at different significance level at LHeC with luminosity projections 100 fb^{-1} (left) and 1 ab^{-1} (right).

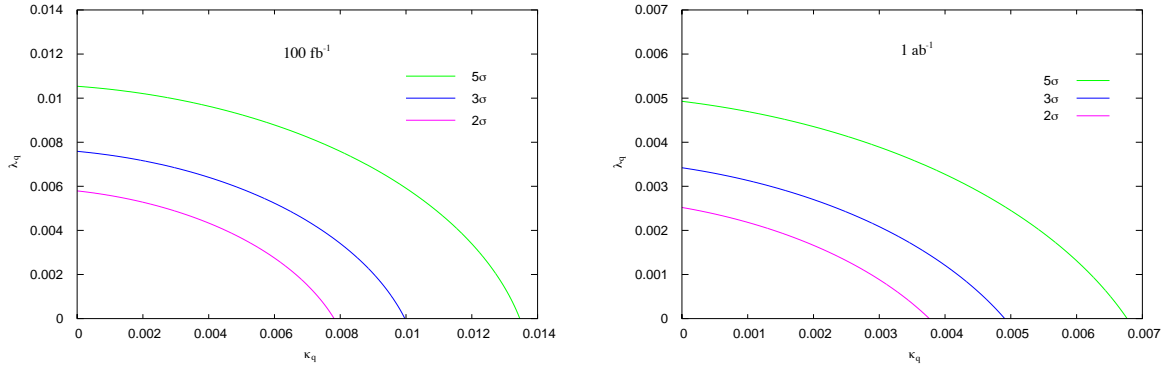


FIG. 16. The reach of proposed couplings at different significance level at FCC-he with luminosity projections 100 fb^{-1} (left) and 1 ab^{-1} (right).

luminosity of $L_{int} = 1 \text{ ab}^{-1}$. The FCC-he with higher center of mass energy of 3.5 TeV will allow us to significantly improve the sensitivity to the top quark FCNC.

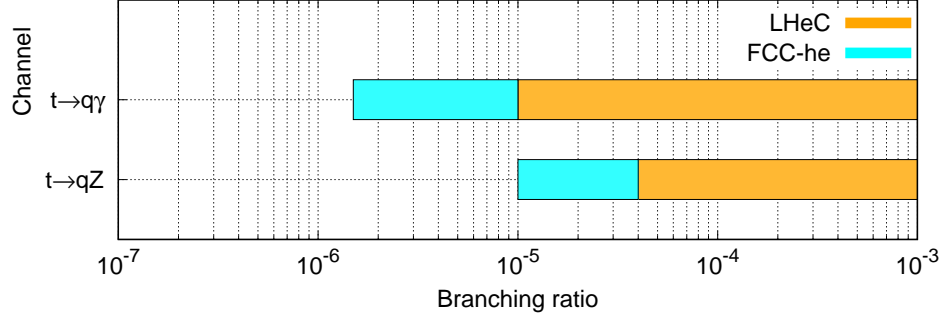


FIG. 17. Summary of branching ratio limits for top quark FCNC decay channels at the future ep colliders LHeC and FCC-he for a luminosity projection of 1 ab^{-1} .

V. ACKNOWLEDGEMENT

This work was partially supported by Bolu Abant Izzet Baysal University Scientific Research Projects under the Project no: 2018.03.02.1286.

-
- [1] N. Cabibbo, Phys. Rev. Lett. **10**, 531 (1963).
 - [2] M. Kobayashi and T. Maskawa, Prog. Theor. Phys. **49**, 652 (1973).
 - [3] S. L. Glashow, J. Iliopoulos and L. Maiani, Phys. Rev. D **2**, 1285 (1970).
 - [4] ATLAS Collaboration, Eur. Phys. J. C **76**, 55 (2016).
 - [5] CMS Collaboration, Journal of High Energy Physics **04**, 035 (2016).
 - [6] M. Aaboud *et al.*, ATLAS Collaboration, Journal High Energy Phys. **1710**, 120 (2017).
 - [7] A.M. Sirunyan *et al.*, CMS Collaboration, JHEP **1707**, 003 (2017).
 - [8] ATLAS Collaboration, ATLAS Note ATL-PHYS-PUB-2013-007 (2013).
 - [9] ATLAS Collaboration, ATLAS Note ATL-PHYS-PUB-2016-019 (2016).
 - [10] J.A. Aguilar-Saavedra, Eur. Phys. J. C **77**, 769 (2017).

- [11] J.L. Abellera Fernandez *et al.*, LHeC Study Group, Journal of Physics G: Nuclear and Particle Physics, vol. **39**, Article ID 075001 (2012).
- [12] More information is available on the FCC web site: <https://fcc.web.cern.ch>.
- [13] I. Turk Cakir, A. Yilmaz, H. Denizli, A. Senol, H. Karadeniz and O. Cakir, Advances in High Energy Physics, vol. **2017**, 1572053, 1-8 (2017).
- [14] H. Denizli, A. Senol, A. Yilmaz, I. Turk Cakir, H. Karadeniz, O. Cakir, Phys. Rev. D **96**, 015024 (2017).
- [15] M. Kumar *et al.*, Phys. Lett. B **764**, 247 (2017).
- [16] C.S. Li, R.J. Oakes, and T.C. Yuan, Phys. Rev. D **43**, 3759 (1991).
- [17] M. Tanabashi *et. al.* (Particle Data Group), Phys. Rev. D **98**, 030001 (2018).
- [18] J. Alwall, M. Herquet, F. Maltoni, O. Mattelaer, and T. Stelzer, Journal of High Energy Physics, vol. **06**, 128 (2011).
- [19] A. Alloul, N. D. Christensen, C. Degrande, C. Duhr, and B. Fuks, Computer Physics Communications, vol. **185**, no. 8, pp. 2250–2300 (2014).
- [20] T. Sjostrand, S. Mrenna, and P. Skands, “PYTHIA 6.4 physics and manual,” Journal of High Energy Physics, vol. **5**, article 026, (2006).
- [21] J. de Favereau *et al.*, Journal of High Energy Physics, vol. **2014**, article 57 (2014).